A&A manuscript no.
(will be inserted by hand later)

Your thesaurus codes are:
11.01.2;11.17.2 quasars;11.19.1

ASTRONOMY
AND
ASTROPHYSICS
17.9.1999

Structure of the Broad-Line Region of 3C 273 ⋆

M. Dietrich[1], **S.J. Wagner**[1,2], **T.J.-L. Courvoisier**[3,4], **H. Bock**[1], **and P. North**[5]

[1] Landessternwarte Heidelberg, Königstuhl, D-69117 Heidelberg, Germany
[2] MSSSO, Private Bay, Weston, ACT 2611, Australia
[3] INTEGRAL Science Data Centre, Chemin d'Ecogia 16, CH-1290 Versoix, Switzerland
[4] Geneva Observatory, CH-1290 Sauverny, Switzerland
[5] Institut d'Astronomie de l'Université de Lausanne, Observatoire, CH-1290 Chavannes-des-Bois, Switzerland

Received 5 January 1999; accepted 17 September 1999

Abstract. The number of discrete emitters in broad-line region cloud models of active galactic nuclei is still unknown. A finite number of clouds will cause intrinsic fluctuations in the emission line profiles. We observed the quasar 3C 273 with high spectral resolution (R$\simeq$10 km s^{-1}) and high signal to noise ratio to estimate the number of individual emitters in the broad-line region. The residua of the emission-line wings of the low ionization lines Hα and Hβ were cross-correlated. We compared the results of the cross-correlation analysis with models of different cloud distributions. The smoothness of the line profiles implies lower limits to the number of individual clouds and to the width of the line profiles of these clouds. For emitters with a line profile width of FWHM$\simeq$ 15 km s^{-1} corresponding to a temperature of $T_e \simeq 2\,10^4$ K, we found that the number of clouds is larger than $N_{cl} = 10^8$. For clouds of significantly larger individual profile width (FWHM$\simeq$ 100 km s^{-1}) it is found that the number of clouds can be of the order of $N_{cl} \approx 10^8$. Since the number of individual emitters is several orders of magnitude larger than the number of stars involved in bloated star models these models can be ruled out as dominant source for broad-line region clouds. However, the non-detection of a cross-correlation signal is consistent with BLR models which assume a continuous hydrodynamical flow as source of the line emitting material.

Key words: quasars: individual (3C 273) — galaxies: emission line profiles — active galactic nuclei

1. Introduction

It is generally believed that the width of the broad emission line profiles reflects the velocity dispersion of the line emitting gas within the broad-line region (BLR) (cf. Blandford & Rees 1992; Osterbrock 1993). The relative strengths of various optical and ultraviolet broad emission lines are consistent with dense cold gas ($n_e \simeq 10^{9\cdots11}$ cm^{-3}, $T_e \simeq 2\,10^4$ K) photoionized by the central continuum source (Ferland & Persson 1989; Ferland et al. 1992). The filling factor of the BLR is estimated to 10^{-6} only (e.g. Netzer 1990). This tiny filling factor motivated a class of BLR models which assume that the line emitting material is confined to an ensemble of numerous discrete clouds moving around the central black hole. But the number of these individual emitters is still unknown as well as their origin and nature. The mass of the clouds is of the order of $10^{-7\cdots-8}$ $M_\odot$ (Peterson 1997). This is much too small to be self-gravitating and a cloud will be evaporated on much shorter time scales than the crossing time, i.e. a few weeks (cf. Krolik 1999). Hence, the necessary confinement mechanism is a major problem of discrete cloud models. Several confinement mechanisms have been proposed for the cloud model e.g. a hot intercloud medium (Krolik, McKee, & Tarter 1981), magnetic fields (Rees 1987), magnetically driven winds (e.g. Emmering, Blandford, & Shlosman 1992; Bottorff et al. 1997), or externally irradiated atmospheres of giant stars of the central star cluster (e.g. Norman & Scoville 1988; Kazanas 1989; Alexander & Netzer 1994, 1997).

Alternative to scenarios of discrete emitters several BLR models have been suggested which base on accretion disk winds, hydrodynamical flows, and the shock interaction of a disk wind and the wind of the central continuum source (e.g. Smith & Raine 1985, 1988; Pelletier & Pudritz 1992; Cassidy & Raine 1993; Murray & Chiang 1995, 1997; Murray et al. 1995). These models solve the confinement problem with a continuous distribution of line emitting material which is embedded in a hydrodynamical flow.

In addition hybrid models have been suggested which based on the interaction of a nuclear wind with obstacles in the close environment of the central engine (e.g. Perry & Dyson 1985; Collin-Souffrin et al. 1988). These models take into account the different properities of high ionization lines (HIL) and low ionization lines (LIL). The LIL are ascribed to accretion disk

Send offprint requests to: M.Dietrich,mdietric@lsw.uni-heidelberg.de
⋆ Based on observations collected at the European Southern Observatory, La Silla, Chile

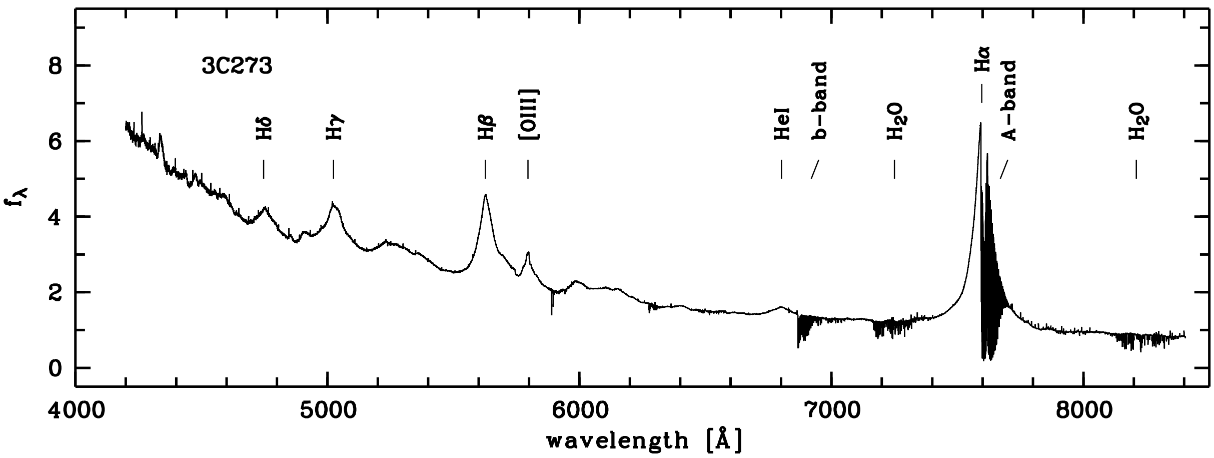

Fig. 1. Average spectrum of 3C 273 — The spectral resolution is $\Delta v \approx 10$ km s^{-1}. The flux f_λ is given in units of 10^{-14} erg s^{-1} cm^{-2} Å^{-1}. The strong contamination of atmospheric absorption bands especially of the red wing of Hα (A-band) is clearly visible.

emission while the HIL are originating in cooling shocked gas which moves around obstacles in the quasar wind.

The number of clouds, N_{cl}, is an important parameter in BLR cloud models. Early estimates of the number of BLR clouds were presented by Capriotti et al. (1981) and Atwood et al. (1982). They studied the line profiles of Seyfert galaxies with high spectral resolution and derived a lower limit of 10^4 to 10^5 individual clouds. Recently, Arav et al. (1997, 1998) estimated the number of BLR clouds to be at least of the order of $N_{cl} \simeq 10^7$.

We observed the luminous quasar 3C 273 to test the BLR cloud model with respect to signatures of a finite number of emitters. Assuming that each cloud contributes in a comparable way to the total line flux, it can be expected that the finite number of clouds will introduce a microstructure in the line profiles. These intrinsic fluctuations will be most prominent in the wings due to the smaller number of clouds in comparison to the line core. This intrinsic scatter can be separated from the observational noise using spectroscopy with high S/N ratio and a spectral resolution of order of $\Delta v \simeq 10$ km s^{-1}.

In Section 2 we will describe the observations and the data reduction of the 2 D echelle spectrograms. In Section 3 the analysis of the line profiles will be presented. The residua of the outer wings have been studied with cross-correlation techniques. For the interpretation of the results of the cross-correlation analysis we developed simplified models assuming a uniform cloud population. The detection of characteristic structures was restricted to emitters with FWHM$\leq$200 km s^{-1}. The details of the model calculations will be described in section 3.

The results of our study will be presented in section 4. In the frame work of a discrete cloud model we estimate a lower limit for the number of individual emitters. We find for the luminous quasar 3C 273 that the number of BLR clouds will be of the order of at least $N_{cl} \simeq 10^8$ based on the analysis of the broad emission-line wings of the Hα and Hβ profile.

The results will be discussed and compared with current cloud models (section 5). Our result is in conflict with models assuming individual emitters e.g. with the number of $N_{bs} \simeq 5\,10^4$ as predicted by detailed bloated star models (Alexander & Netzer 1994).

For the class of disk wind models and hydrodynamical flows the emission line profiles are expected to be smooth. Therefore, these models can not be studied with the method we apply to test the discrete cloud BLR models.

2. Observations and Reduction

We observed the quasar 3C 273 with the 3.5 m NTT at La Silla/ESO with EMMI REMD in February 1996. Echelle grating #10 and grism 3 as cross-disperser were used to obtain echelle spectra of this quasar. The pixelsize of 24μm of the 2 k CCD device (CCD #36) corresponds to 0.″27 / pixel projected onto the sky. The slit width was set to 1″ while the slit length was restricted to 4″ to avoid order overlap in the blue wavelength range of the 2 D echelle spectrograms. The position angle of the slit was optimized for each object exposure to minimize the light loss due to the differential refraction. During the first night the seeing varied between 0.″6 and 1.″0 while it was nearly constant during the second night (0.″6). For flux calibration we observed several standard stars — HR 3498, HR 4681, μ Col, ζ Pup, ϑ Crt, and ϵ CMa. These stars were reduced in the same way as the spectra of 3C 273.

The 2 D echelle spectrograms were bias and dark corrected in the standard manner. Next the echelle spectra were corrected with respect to the straylight component making use of the interorder sections. Generally, the tracing of the individual echelle orders can be obtained from the measurement of a bright star. For the current observations the pattern of the echelle orders was not only shifted perpendicular to the order number as it is expected for a fixed order pattern but an additional individual stretching factor was detected increasing to short wavelengths. Hence, the location of the individual orders had to be determined for each object separately. The 2 D echelle spectrograms were flatfield corrected using the average of 11 dome flatfield exposures. Several ThAr echelle spectra were observed for wavelength calibration. The wavelength shift between the individual exposures is less than 0.01 pixels and was neglected. The dispersion in the red part of the spectrum amounts to 0.08 Å/pxl and in the blue part to 0.05 Å/pxl. The rms of the fit to the detected ThAr emission lines was 0.009 Å. The wavelength scale of the individual echelle orders was set to a uniform scale of 0.05 Å/pxl. The dispersion of the echelle spectrograms was determined from several night sky lines. We measured a value of FWHM = (0.194±0.006) Å corresponding to $\Delta v \simeq 10\,\mathrm{km\,s^{-1}}$.

Table 1. Observing log of 3C 273

date	UT_{start}	t_{int}	date	UT_{start}	t_{int}
Feb., 11	04:21:53	60 min	Feb., 12	04:28:28	75 min
Feb., 11	05:29:54	60 min	Feb., 12	05:50:40	75 min
Feb., 11	06:37:06	60 min	Feb., 12	07:15:38	60 min
Feb., 11	07:44:17	60 min			

The spectrum of 3C 273 was extracted from the 2 D echelle spectrograms with an aperture size of 1″ x 2.″4. The individual orders were flux calibrated with a sensitivity function which we derived from the standard stars. These stars had been observed with the same setup as 3C 273. The flux calibrated orders of 3C 273 spectra were merged to a continuous spectrum with an order overlapp of 5 Å yielding a total wavelength coverage of 4200 Å — 8400 Å.

The individual 1 D spectra of 3C 273 were corrected for cosmic ray events. Each spectrum was compared with the other spectra. The criterium for a cosmic ray event detection was given by a 3-σ threshold which was estimated from several non contaminated regions of a spectrum. If the flux of an individual wavelength element deviated more than 3-σ from the median of the comparison spectra the flux was replaced by the median given by the other spectra.

Finally, the individual spectra of 3C 273 were merged to a mean spectrum of higher signal-to-noise ratio. The flux of each wavelength element of the seven spectra were ordered by strength. The lowest and highest value were excluded and the mean of the remaining 5 values was calculated. If the excluded flux values differed by more than 3-σ from this mean they were replaced by the mean otherwise they were taken into account calculating the average flux the the corresponding wavelength element.

The signal-to-noise ratio of the emission line profiles in the outer wings of Hα and Hβ was estimated for a region corresponding to $(-6000 \;...\; -5000)\,\mathrm{km\,s^{-1}}$. The signal-to-noise ratio of the individual spectra is of the order of ≈60 for Hα and Hβ and ≈150 for the mean spectrum. We fitted a power law continuum to the spectra to estimate the signal-to-noise ratio for the emission-line flux alone. We estimated a value of $S/N_{H\alpha} \simeq 35$ and $S/N_{H\beta} \simeq 15$ for the emission-line profile wings of the average spectrum.

3. Analysis of Emission Line Profiles

3.1. Preparation of the observed line profiles

Proper parts of the wings have to be selected before the line profiles of Hα and Hβ can be studied for intrinsic fluctuations. In addition to instrumental effects the contribution of several emission lines like [OI]6364, [SII]6717,6731, [OIII]4959, and HeII4686 have to be estimated. Furthermore, the influence of atmospheric features in absorption or in emission have to be investigated carefully. The strongest absorption feature in the red part of the spectrum is the A-band due to O_2. The red wing of the Hα profile of 3C 273 is strongly contaminated by this atmospheric absorption (Fig. 1). At wavelengths larger than 8100 Å the spectrum is strongly influenced by H_2O absorption. Another prominent H_2O absorption contaminates the spectrum at the blue side of the Hα line profile. These absorption line doublets can be detected at a level of less than 1 % up to $\lambda \approx 7415$ Å in the blue wing corresponding $\Delta v \approx -7200\,\mathrm{km\,s^{-1}}$ with respect to the line center of Hα.

We detected several weak emission lines in the blue wing of the Hα line profile which are due to Meinel rotation-vibration bands of OH (Osterbrock & Martel 1992; Osterbrock et al. 1996). The width of these weak night sky emission-lines corresponds to FWHM $\simeq 10\,\mathrm{km\,s^{-1}}$. The range of the contamination free part of the blue wing of the Hα emission line profile is given by the location of these OH emission lines (Table 2). In the blue wing of the Hβ line profile we detected three narrow emission lines at λ=5506.144 Å, 5560.043 Å, and 5577.338 Å. The last emission line was identified as [OI]5577. In the outer blue wing of the Hβ profile the influence of the HeII4686 emission line is visible up to $\Delta v \approx -7000\,\mathrm{km\,s^{-1}}$. The outer red wing of the Hβ line profile is contaminated by [OIII]4959 emission.

Table 2. Detected Meinel rotation-vibration bands of OH in the blue wing of the Hα line profile of 3C 273

feature	λ [Å]	feature	λ [Å]
8-3 P2 (5.5)	7429.781	4-0 R1(2.5)	7473.678
8-3 P1e(6.5)	7438.243	4-0 R1(1.5)	7483.476
8-3 P1f(6.5)	7438.702	4-0 R2(0.5)	7493.670

Because the Hα line profile is strongly contaminated from atmospheric A-band absorption we will concentrate entirely on the blue wing of Hα and Hβ line profile.

The profiles of the Hα and Hβ line were transformed into velocity space (z = 0.1576) for better comparison of corresponding parts (Fig. 2). The redshift was determined from the Hβ emission line.

The line profiles were prepared for the analysis following the method suggested by Tonry & Davis (1979). First, polynomials of 8$^{\mathrm{th}}$ order were fitted to the blue wing of the line profile

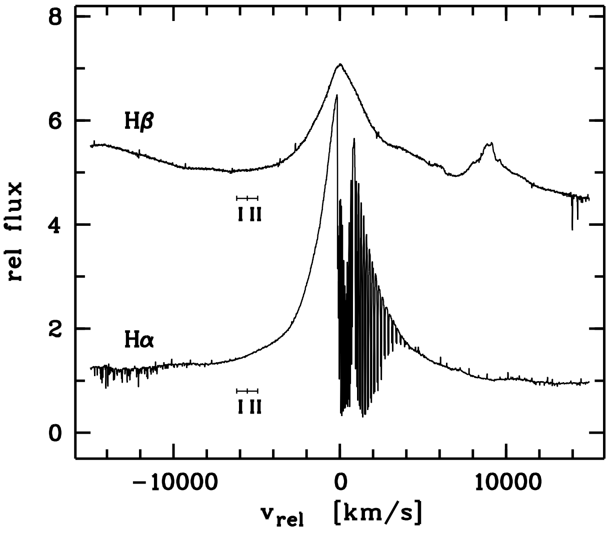

Fig. 2. The Hα and Hβ emission line profile transformed into the rest-frame of 3C 273 (z=0.1576). Section I and II which we used for the cross-correlation analysis are indicated by the horizontal bars.

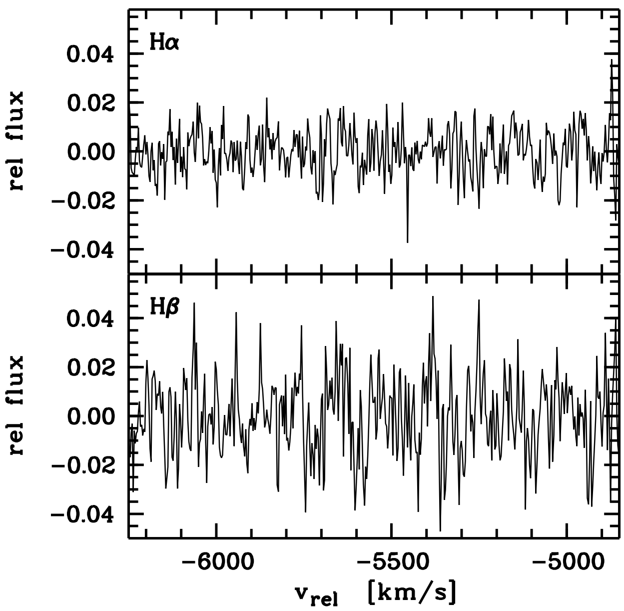

Fig. 3. The residuum of the blue wing of the Hα line profile is shown in the top panel and the corresponding residuum of the Hβ line is displayed in the bottom panel.

in the range (-8000 ... -1000) km s^{-1}. The resulting residua were corrected for low frequency variations. Therefore, they were transformed into Fourier space, frequencies corresponding to structures wider than 200 km s^{-1} were suppressed, and subsequently re-transformed to velocity space. In addition we analysed the residua which were not corrected for low frequency structures to allow the detection of wider features. Finally, the start and end of the residua were damped with a function f(x) = 0.5(1-cos(xπ/f N)). The extent of the residua in velocity space should be at least of the order of Δv$\approx$500 km s^{-1}. We studied two parts of the residua which are not contaminated by the absorption and emission features which were detected in the profile wings (Table 2). The parts which we used for the cross-correlation analysis range from v = -6200 to -5568 km s^{-1} (section I) and v = -5568 to -4941 km s^{-1} (section II), respectively (Fig. 2).

3.2. Cross-Correlation Analysis

A finite number of discrete emitters will cause characteristic fluctuations in the line profiles. Cross-correlation techniques offer a straightforward way to search for similar microstructures. In the optically thin case the profile of different emission lines of a single cloud will be identical. Therefore, cross-correlation of corresponding parts of the residua of two line profiles will lead to a cross-correlation function peak at v = 0 km s^{-1}. In the case of very optically thick emission lines optical depth effects will cause different profile shapes of e.g. the Hα and Hβ line since most of the flux is emitted in the wings (e.g Davidson & Netzer 1979). This will result in symmetrically located peaks around v = 0 km s^{-1} at v$\approx$ $\pm$10 km s^{-1} and v$\approx$ $\pm$80 km s^{-1} in the cross-correlation function assuming $\tau_{\mathrm{H}_\alpha} \simeq$150 (Atwood et al. 1982).

We used the interpolating cross-correlation method (cf. Gaskell & Peterson 1987; White & Peterson 1994) to calculate the cross-correlation function (ICCF). In the first pass the discrete points of the first input file were correlated with the linearly interpolated second input file. In the second pass the discrete points of the second input file were correlated with the linearly interpolated first input file. Both cross-correlation functions were averaged. The ICCF method was applied to the residua of the Hα and Hβ line profile.

3.3. Model Simulations

We studied simple models to derive an estimate how many individual clouds can be hidden in a line profile with a given S/N ratio.
It was assumed that the profile of a single cloud can be described by a Gaussian. If the width of the emission-line profile of a single cloud is caused by thermal broadening alone, a FWHM of 15 km s^{-1} and 25 km s^{-1} corresponds to a temperature of $T_e \simeq 10^4$ K and 5 10^4 K, respectively. If the line width of a single cloud is of the order of 50 km s^{-1} to 200 km s^{-1} thermal broadening alone is not sufficient to produce such broad profiles since the corresponding temperatures are too high, ranging from $T_e \simeq$2 10^5 K to $T_e \simeq$4 10^6 K. This is in contradiction with photoionization models. Hence, additional mechanisms are necessary to produce broad line profiles. In this context it is possible that internal turbulence of the line emitting material is important. Furthermore, large optical depth will introduce a broadening proportional to $\sqrt{\ln\tau}$ (cf. Davidson & Netzer 1979). If the clouds are very optically thick ($\tau_{\mathrm{H}\alpha} \simeq$

10^4) the profiles are broadened by a factor of $\sim$3 due to the large optical depth. Another process to cause broader emission lines is scattering in a sphere of free electrons enveloping each individual cloud (e.g. Bottorff et al. 1997). Furthermore, it was assumed that all clouds had the same FWHM. We computed cloud ensembles of different individual line widths, in particular FWHM = 15, 25, 50, 75, 100, 200 km s^{-1}, i.e. our analysis was restricted to individual structures with FWHM$\leq$200 km s^{-1}.

The line emission of a discrete cloud was taken as isotropic. This is a strong simplification since the dominant fraction of the cloud population is optically thick and hence the line emission will be strongly anisotropic (e.g. Ferland et al. 1992). Furthermore, Baldwin et al. (1995) showed that BLR clouds with widely different properties process the ionizing continuum with locally optimal efficiency. The radial dependence of the cloud luminosity should be less than 1/r^2 otherwise the profiles show wings which are too strong. We computed models with a radial dependence of L_{cl}=const, $\sim$1/r, $\sim$1/r^2.

The locations of the discrete clouds were randomly selected within a three-dimensional sphere. Furthermore, we assumed that the clouds are moving on closed orbits around the central black hole. Bradley & Puetter (1986) investigated models of discrete emitters on bounded orbits. Clouds moving on Keplerian orbits with high excentricity yielded profiles which correspond to observed AGN broad emission line profiles. Within these models it was shown that aspect effects caused by optically thick clouds do not play such an important role as had been claimed by Hubbard & Puetter (1983).

We computed the following simple cloud distributions.

a) The clouds were distributed randomly in velocity space following a Gaussian distribution. A Gaussian velocity distribution is characteristic for objects deep within the nuclei of giant elliptical galaxies (Sargent et al. 1978; Harms et al. 1994). The velocity dispersion of the cloud ensemble was set to FWHM = 3000 km s^{-1} to correspond to the width of the Balmer Hα and Hβ emission lines of 3C 273.

b) The individual clouds are moving on randomly orientated Keplerian orbits around a massive black hole filling a spherical volume. The distribution of clouds shows a higher concentration with respect to the plane perpendicular to the sky plane (Fig. 4). Such a distribution has been selected since it is generally assumed that the individual emitters are arranged in a more flattened geometry than in a homogeneous spherical one (cf. Osterbrock 1993). The mass of the black hole was set to $M_{\rm bh} = 10^8\,M_\odot$. The distance of the clouds to the central energy source was restricted to $r_{\rm in} = 0.1$ light days and $r_{\rm out} = 100$ light days.

c) The same model as (b) but the luminosity of the cloud varies with the distance to the central continuum source as r^{-1}

d) The same model as (b) but the luminosity of the cloud varies with the distance to the central continuum source as r^{-2}

e) The same model as (b) but the ionizing radiation is concentrated within a bi-conical beam with an opening angle of 30°. The bi-conical structure is 30° out of the line of sight and inclined by 60° with respect to the sky plane. In this model only those clouds contribute to the line flux which are inside of the bi-conical structure.

With the exception of models (c) and (d) the clouds were treated as identical emitters. The number of clouds for each ensemble ranged from $10^4 \leq N_{cl} \leq 10^9$. Photon noise was added to the calculated line profiles to simulate S/N ratios ranging from S/N = 10 to S/N = 200. For each combination of N_{cl}, FWHM of an individual cloud, and S/N ratio, 10 models were computed. We assumed a line ratio of Hα/Hβ = 3.0 to calculate model Hα and Hβ profiles. The photon noise which was added to the profiles was computed independently for each profile bin. The model line profiles were treated in the same way as the real observations to calculate residua and cross-correlation functions. The parts of the residua which we took to calculate the cross-correlation function were selected taking into account that the relative flux is comparable to the flux of the observed profile sections.

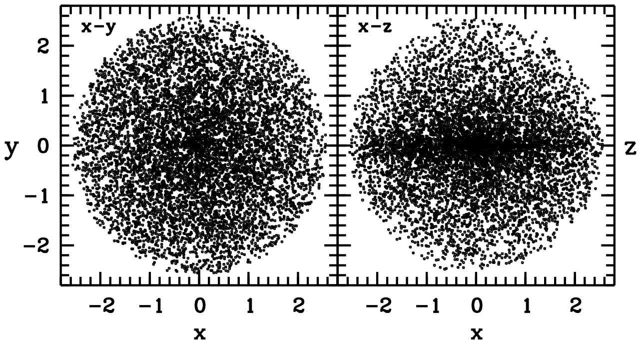

Fig. 4. Distribution of individual emitters with $N_{cl}=10^4$. The projection in the x-y plane shows a homogeneous distribution. However, the projection of the cloud locations in the x-z plane displays a slightly higher concentration of clouds with respect to the x-y plane.

4. Results

The residua of the mean Hα and Hβ profile as well as of the individual spectra were investigated for intrinsic microstructure. Hence the line profile residua were cross-correlated to search for peaks in the ICCF. To estimate the significance of a CCF peak we calculated a 3-σ threshold. The 1-σ level was given by the r.m.s. of the ICCF for a velocity range of Δv=$\pm$500 km s^{-1}. The results of the cross-correlation analysis of the Hα and Hβ residua of the mean spectrum of 3C 273 (section I and II) are displayed in Figure 5. The inner dotted lines indicate the 1-σ level while the outer dotted lines show the 3-σ threshold. The ICCF of both sections show no significant ICCF peak. However, there is a marginal indication for a 2-σ detection at v$\simeq$-25 km s^{-1}. The ICCF was also calculated using the line profile residua of the seven individual spectra of 3C 273. The cross-correlation analysis yields for each section 49 individual ICCFs. For example the section I residuum of the Hα wing of spectrum 1 was cross-correlated with the corresponding Hβ residuum of all of the individual spectra. The ICCFs of the individual residua were averaged separately for both sections. This yielded two average ICCFs for the Hα and Hβ line profile residua. These average ICCFs and the corresponding 1-σ and 3-σ threshold are presented in Fig. 6.

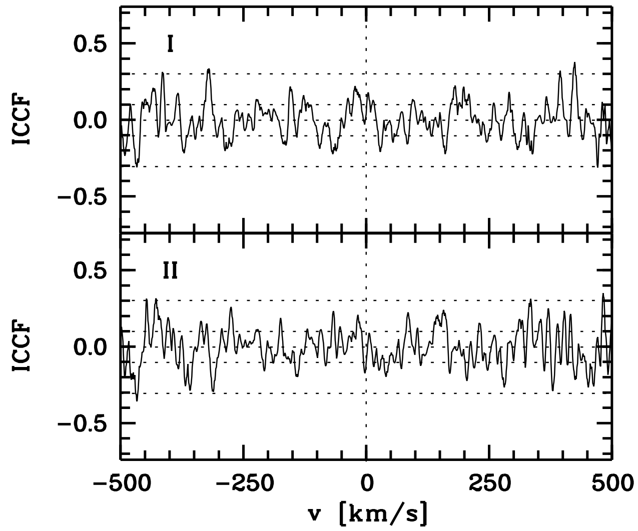

Fig. 5. The ICCFs of cross-correlating the Hα and Hβ residua of the mean spectrum (section I and II given in 3.1). The dotted horizontal lines indicate the 1-σ and 3-σ threshold.

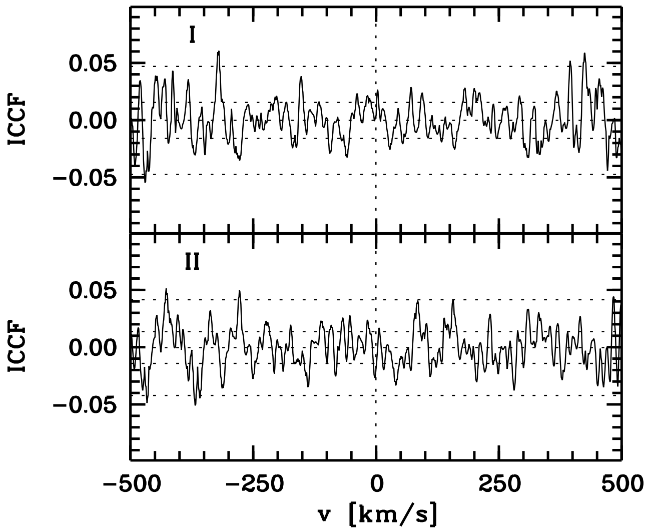

Fig. 6. The averaged ICCFs of cross-correlating the Hα and Hβ residual sections of the individual spectra.

The ICCF of section I and II calculated for the mean Hα and Hβ profile residua (Fig. 5) and given as the average of the ICCFs the individual line profile residua (Fig. 6) are nearly identical. Both show the same ICCF features and relative position of the 1-σ and 3-σ level. But the amplitude of the average ICCF is nearly an order of magnitude smaller than the ICCF of the mean spectrum. Furthermore, the marginal feature at v$\simeq$-25 km s^{-1} in the mean ICCF of section I is less prominent in the average ICCF of section I. These four ICCFs provide evidence that there is no significant feature in the ICCF of section I and II.

The Hβ and Hα emission line profiles are not identical. It is known that the Hβ profile is broader than the Hα profile (e.g. Crenshaw 1986). Hence it is possible that the dominating cloud population of the Hβ emission is not the one that give rise to most of the Hα emission and vice versa. If this is the case the null cross-correlation signal between these two lines will be difficult to interpret. Furthermore, an individual cloud will have a different optical depth for Hβ and Hα which cause small differences in the intrinsic emission line profiles for these lines for a single cloud. A way to avoid these problems is to cross-correlate two different epochs of the same emission line profile. Therefore, we correlated the Hα and the Hβ line profile residua independently. The individual residua were taken to calculate the ICCF of the blue wing of Hα versus Hα as well as the blue wing of Hβ versus Hβ. Weak night sky emission lines or absorption features would introduce correlation peaks in the ICCF which might be misleading. Hence, in this case it is very important to use only those parts of the residuum which are not contaminated.

Each part of the residuum of the Hβ line as well as of the Hα line can be compared with the corresponding part of the six other spectra. This procedure yields for each section 21 ICCFs. The average ICCFs of the two parts of the Hα and Hβ residuum are shown in Fig. 7. The dotted horizontal lines indicate the 1-σ and 3-σ level which were computed in the same way as described above. There is no indication for a significant signal in the ICCF of the Hα or Hβ line profile residua. Furthermore, there is no spurious narrow peak at v$\simeq$0 km s^{-1} which might be attributed to weak night sky emission or absorption features. It will not be possible to detect structures wider than FWHM $\simeq$ 200 km s^{-1} using the residua of the observed spectrum corrected for low frequency structures. It seems not to be very realistic that the line width of individual emitters is due entirely to thermal broadening but electron scattering and optical depth effects can provide additional broadening mechanisms. We cross-correlated the uncorrected residua of the Hα and Hβ line profiles, too (Fig. 8 and 9) to allow for the detection of possible wider structures of the order of FWHM $\simeq$ 600 km s^{-1}. This limit was given by the width of the sections which we analysed for the Hα and Hβ residua.

The ICCFs of both sections show the same features and strength independently of the correction for low frequency structures. This result indicates that structures wider than FWHM $\simeq$200 km s^{-1} do not have strong influence on the microstructure of the line profile.

Finally, we have calculated the auto-correlation function for the individual sections of the residua of the mean Hα and Hβ line profile (Fig. 10). The ACF of the Hβ and Hα residua shows a narrow peak with a width of FWHM = (6.2$\pm$0.7) km s^{-1}. This

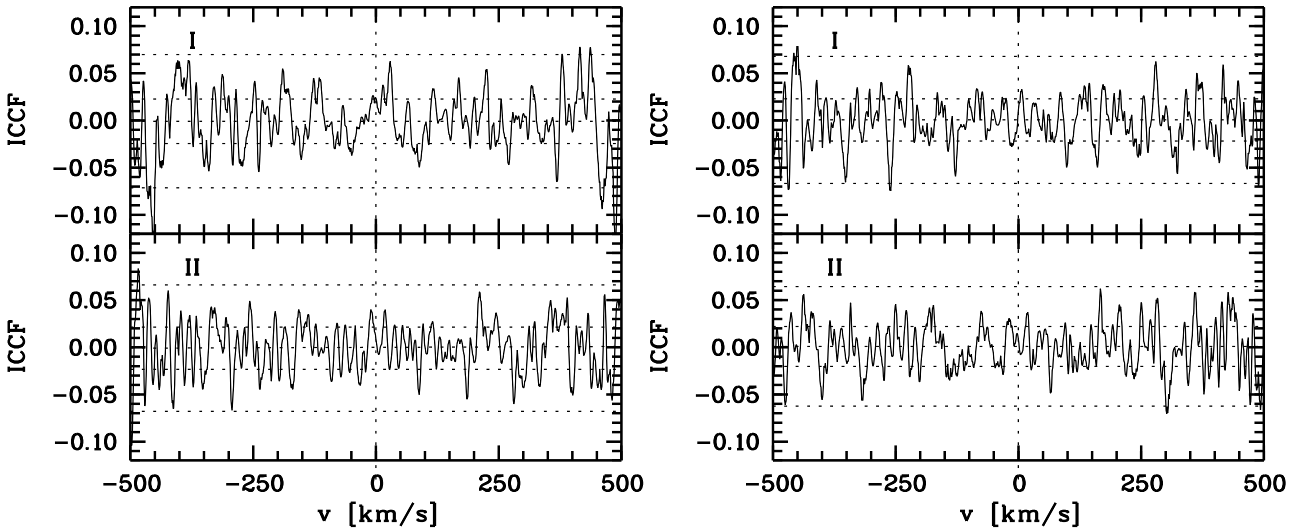

Fig. 7. At the left side the average ICCFs of section I and II are shown which we obtained by cross-correlating the individual Hβ residua. The panels at the right side display the average ICCFs which were calculated for the residua of the individual Hα sections.

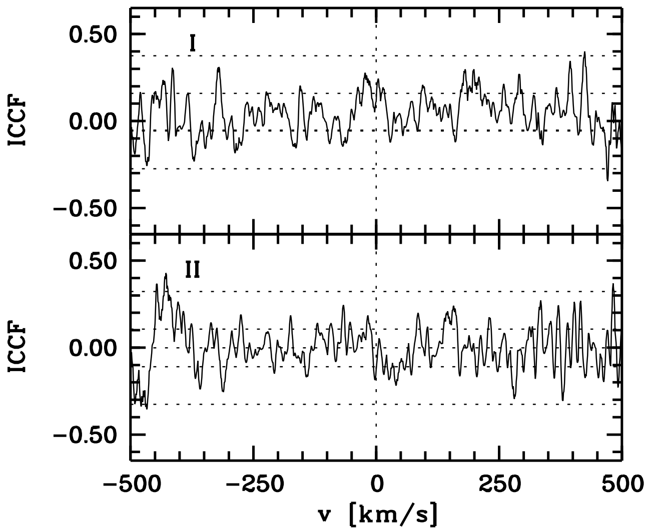

Fig. 8. The ICCFs of the uncorrected Hα and Hβ line profile residua of the mean spectrum. Both ICCFs are nearly identical with the corresponding ICCFs shown in Fig. 5.

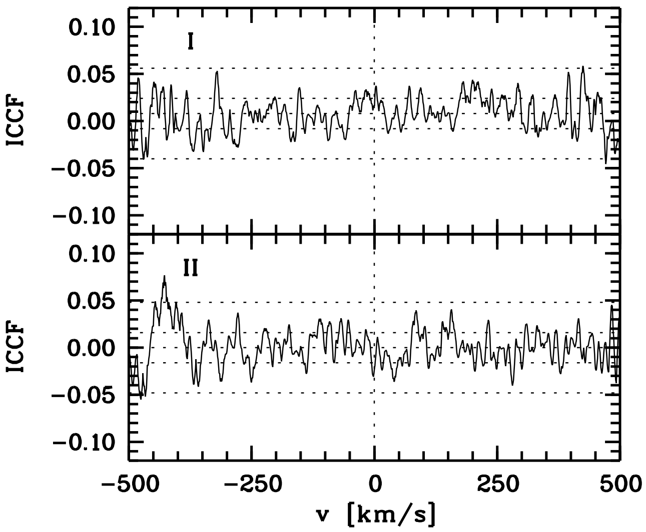

Fig. 9. The averaged ICCFs of the uncorrected Hα and Hβ line profile residua of the individual spectra.

average width of the peak is comparable to the spectral resolution of the echelle spectra.

The cross-correlation analysis of the residua of the Hβ and Hα emission line profiles of 3C 273 provides no evidence for a significant signal in the ICCF which can be ascribed to intrinsic fluctuations of the line profile. This result is valid for cross-correlating the Hα vs. Hβ residua as well as cross-correlating Hα vs. Hα and Hβ vs. Hβ and it is also independent with respect to the correction of low frequency structures.

5. Discussion

The cross-correlation analysis of the residua of the Hα and Hβ line profiles of 3C 273 provides no evidence for an intrinsic microstructure. No significant feature was detected in the ICCFs which we calculated. The lack of a cross-correlation signal for the ICCFs of the Hα vs. Hβ residua is difficult to interpret since the physical state of an individual cloud will yield different profiles for the Hα and Hβ line profile. However, this problem vanishs in the case of a direct comparison of Hα vs. Hα and Hβ vs. Hβ, respectively.

To use this result for an estimate of the number of individual emitters we studied several simplified scenarios for the cloud

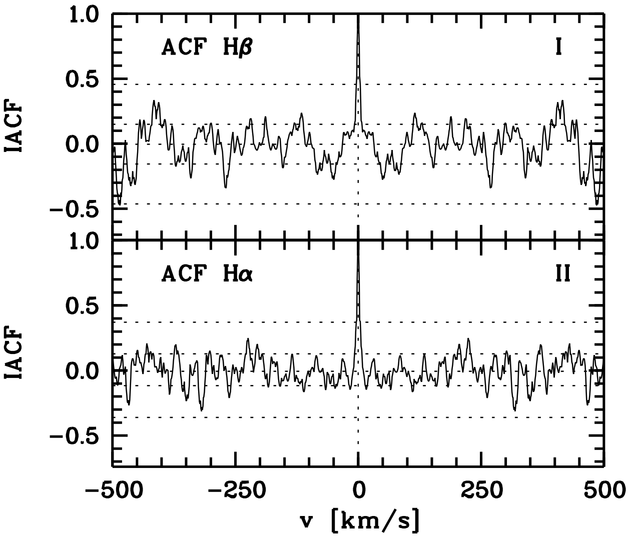

Fig. 10. In the top panel an example of the ACFs calculated for the Hβ residua (section I) is shown while the same is displayed for the Hα residua in the bottom panel.

distribution and cloud properties. It is obviously a very rough assumption to use a unique line profile for the Hα and Hβ emission for an individual cloud. The different optical depth for Hα and Hβ will lead to different line profiles in the case of optically thick clouds which is strongly indicated by the variability of the broad emission lines in AGN. Furthermore, Baldwin et al. (1995) demonstrated that the line emission in a discrete cloud model can be ascribed to locally optimally emitting clouds. Baldwin et al. (1995) suggested that the properties of the line emitting gas are not characterized by a single combination of hydrogen density n$_H$ and ionizing photon flux density ϕ(H). But the conditions for optimal re-processing of the continuum radiation are satisfied for a wide range in the n$_H - \phi$(H) plane. Furthermore, the range is different for different lines. Hence the line profile of different lines are expected to be not unique as assumed in our simple models. For a more realistic simulation of the cloud ensemble it will be necessary to take this into account but this is beyond our current code for model calculations. But the influence of different profiles of different lines can be avoided by investigating the same emission line profile measured at different epochs.

Emission-line profiles were calculated for cloud ensembles consisting of 10^4 to 10^9 discrete emitters. The line width of a single gas concentration varied between 15 km s^{-1} $\leq$ FWHM $\leq$ 200 km s^{-1}. Photon noise comparable to the real data was added to the cumulative line profiles.

The core of the calculated profiles is different from the observed Hα and Hβ profiles of 3C 273 for the Keplerian models which (b - d) show a narrow core structure. However, the cumulative profile of the bi-conical model (e) is similar to the observed line profiles of 3C 273 even though the width is of the order of FWHM$\simeq$1300 km s^{-1}. Since we are more interested in the structure of the outer line-profile wings than in modelling the entire profile the results can be taken as a first estimate of the cloud number. More sophisticated models have to take into account a multi-component distribution of individual emitters as well as anisotropic emission for individual clouds refer to the large optical depth of the line emitting material.

The comparison of the blue wings of the model profiles displays the signature of the different line width of the individual line emitting blocks. The cumulative line-profiles of 10^5 discrete clouds show too much structure in the wings. The intrinsic fluctuations of the line-profile are still stronger than in the observed Hα profile of 3C 273 for N$_{cl}$=10^8 even in the case if the model profiles are characterized by a signal-to-noise ratio of S/N = 30 (Fig. 11). This is especially the case for the bi-conical models which we studied. But the line-profile

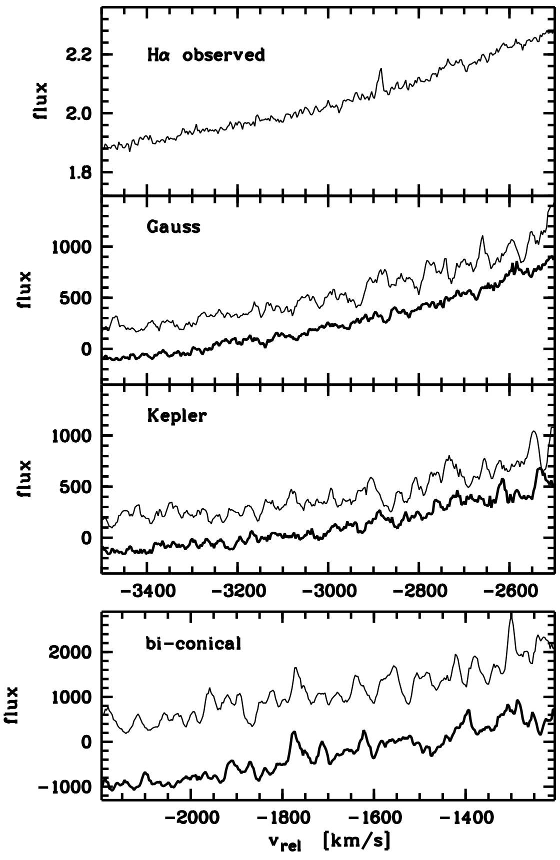

Fig. 11. Comparison of the blue wing of the mean Hα profile of 3C 273 (top panel) with the profiles of the Gaussian (a), the Keplerian (b), and the bi-conical (e) models. An individual emitter has a line width of FWHM = 15 km s^{-1}. The thin line corresponds to N$_{cl}$=10^5 and the thick line to N$_{cl}$=10^8.

wings start to become more similar to the observed profiles if the width of a discrete cloud is of the order of FWHM$\simeq$100 km s^{-1}. While cloud ensembles of N$_{cl}$ $\simeq$$10^5$ clouds still show low amplitude structures of the order of $\sim$200 km s^{-1}, the profile wings of the models are comparable to the observed line profiles if N$_{cl}$ $\simeq$$10^8$ (Fig. 12). However, the bi-conical model

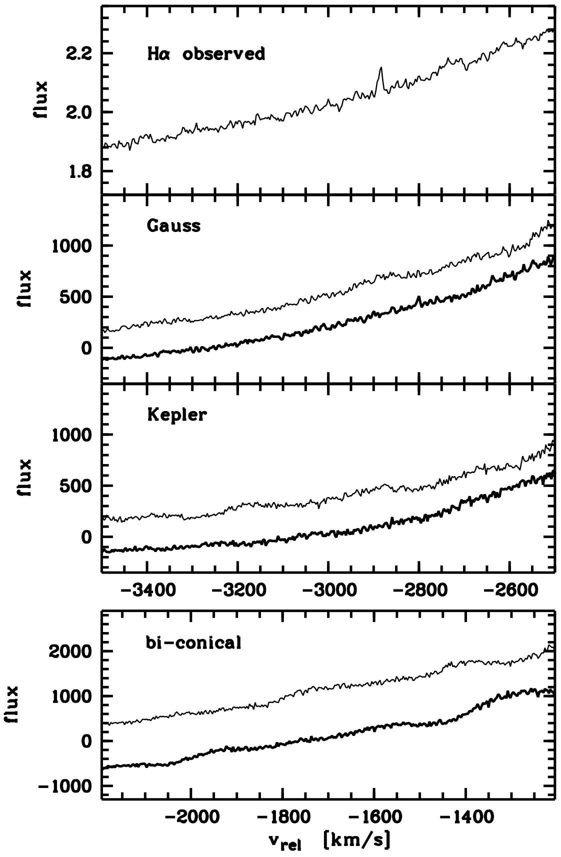

Fig. 12. Comparison of the blue wing of the mean Hα profile of 3C 273 (top panel) with the profiles of the Gaussian (a), the Keplerian (b), and the bi-conical (e) models. The individual emitters have a line width of FWHM = 100 km s^{-1}. The thin line corresponds to $N_{cl}=10^5$ and the thick line to $N_{cl}=10^8$.

still displays some features on larger scales of the order of $\approx$ 100km s^{-1}. This might be due to the orientation of the biconus and the distribution of the clouds (cf. Fig. 4). The fraction of clouds close to the inner boundary of the cloud distribution is smaller than for the spherical distribution (model a-d). Therefore, the number of clouds in the outer wings is smaller yielding slightly more structured profiles.

A line width of FWHM = 15 km s^{-1} corresponds to a temperature of $T_e \simeq 2\,10^4$ K. The structured profiles of cloud ensembles with individual line width of FWHM = 15 km s^{-1} to 25 km s^{-1} yield prominent features in the ICCF. For $N_{cl}=10^5$ the ICCF peak at v = 0 km s^{-1} is of the order of 0.9 and for $N_{cl} = 10^8$ the ICCF peak is higher than the 3-σ threshold (Figs. 13, 14). This result is still valid for individual line widths of FWHM$\simeq$100 km s^{-1} if the total number of clouds is $N_{cl} \simeq 10^5$ (Fig. 15). But in the case of $N_{cl} = 10^8$ the ICCF shows no significant peak at v$\simeq$0 km s^{-1}. However, there is a broad feature indicating the finite number of clouds in the ICCF (Fig. 16).

The results of the ICCF analysis of the model line-profiles were compared with the ICCFs deduced from the observed Hα and Hβ line profiles. No significant ICCF peak is detected for the observed line profiles. If the line width of an individual emitter is of the order of FWHM = 15 km s^{-1} to FWHM = 25 km s^{-1} the number of clouds has to be several orders of magnitude larger than 10^9 to avoid an ICCF peak. If the line width is of the order of FWHM$\simeq$100 km s^{-1} it is possible to hide $N_{cl} \simeq 10^8$ clouds in the line profile. If the line width is due to thermal broadening alone a FWHM = 100 km s^{-1} corresponds a temperature of $T_e \simeq 10^6$ K for the line emitting gas. But this is in serious conflict with current successful photoionization models which indicate a temperature of $T_e \simeq 2\,10^4$ K (cf. Osterbrock 1993; Baldwin et al. 1995; Korista et al. 1997). Therefore, additional mechanisms are necessary to cause the larger line width.

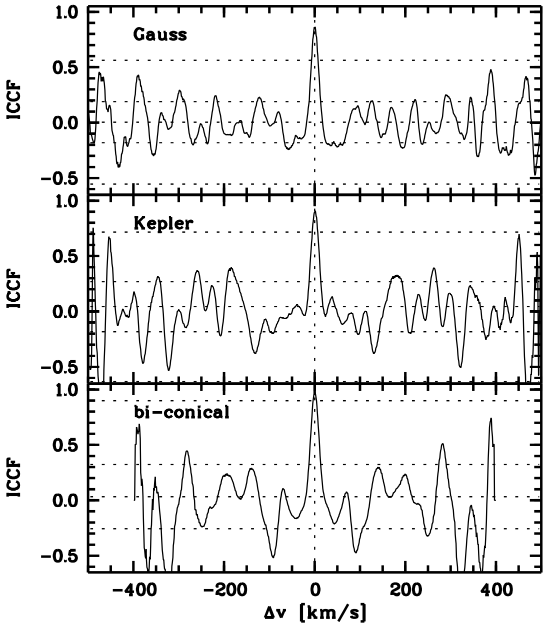

Fig. 13. The corresponding ICCF of a Gaussian (top), Keplerian (middle), and bi-conical model (bottom) for FWHM=15 km s^{-1} ($N_{cl}=10^5$) calculated with the profiles shown in Fig. 11.

Several mechanisms can broaden a line profile in addition to thermal turbulence. Photoionization models and variability studies provide strong evidence for very large optical depth of the line emitting material. The optical depth of Lyα is assumed to be of the order of $\tau_{\mathrm{Ly}\alpha} \simeq 10^6$ which will result to an optical depth of $\tau_{\mathrm{H}\alpha} \simeq 10^4$ for the Hα emission. Since the factor of the line broadening is given by $\sqrt{\ln\tau}$, the line width of the Hα and also of the Hβ line-profile of an individual cloud will be enlarged by a factor of $\sim$3 (cf. Davidson & Netzer 1979).

Another possible mechanism to enlarge the line width is electron scattering. Regardless of whether the emission originates in an accretion disk or in individual gas concentrations it can be assumed that the line emitting region is surrounded by an atmosphere of free electrons (e.g. Emmering et al. 1992; Bottorff

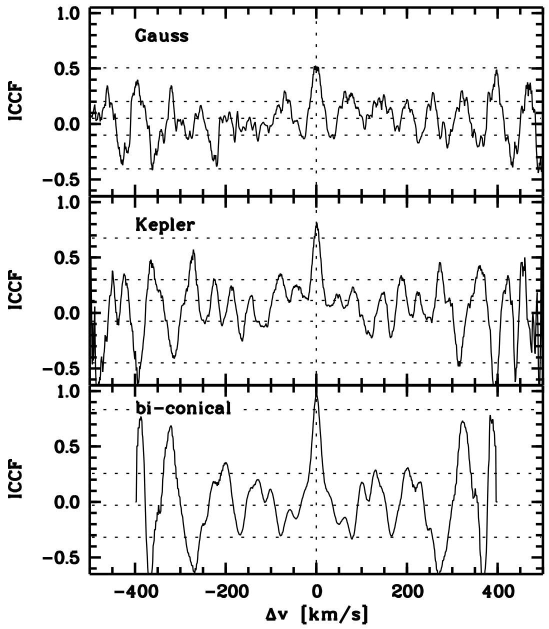

Fig. 14. The same as Fig. 13 for N_{cl}=10^8

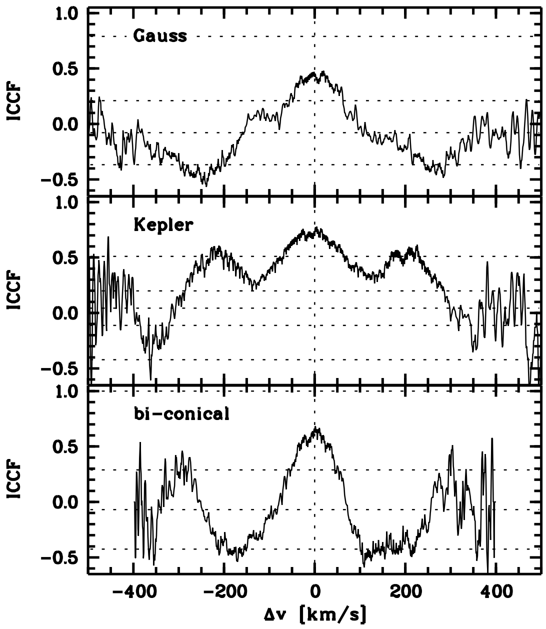

Fig. 15. The corresponding ICCF of a Gaussian (top), Keplerian (middle), and bi-conical model (bottom) for FWHM=100 km s^{-1} (N_{cl}=10^5) calculated with the profiles shown in Fig. 12.

et al. 1997). A fraction of the line photons will be scattered in these atmospheres which will introduce a broad base to the line profile of a single emitter. The width of the broad base will be of the order of FWHM≃500 km s^{-1} assuming that the electron gas can be described with $T_e \simeq 2\,10^4$ K. Broad components in addition to the narrow profile of strong emission-lines have been observed for symbiotic stars for the OVI1034 emission-line (Schmid et al. 1999). We calculated several line profiles for model (a) to (e) assuming a broad base (FWHM=500 km s^{-1}) to investigate the influence of the broadening on the cumulative line profile. The relative fraction of flux contained in the broad base varied between 0.05 to 0.5. The line profiles started to differ significantly from the models without a broad component in the discrete line profile if the relative fraction of the scattered flux is of the order of 50%. This fraction is far too high. In symbiotic stars the fraction of line flux of OIV1034 which is scattered in the broad component is of the order of 5%. Furthermore, if ∼50% of the line photons are scattered by free electrons the scattering medium has to have a too large column density which will reflect much of the incident ionizing flux. This will modify the observed emission-line spectrum. Hence, the influence of a broad component introduced by electron scattering is negligible for a scattered flux fraction of less than 5%.

The ICCF analysis of the model line-profiles indicates that the width of the ICCF peak is related to the line-width of the individual emitters. The ICCFs of the models with widths of FWHM≃100 km s^{-1} for an individual emitter show broad ICCF peaks while the narrow line-profile clouds yield narrow peaks in the corresponding ICCF. The ICCFs of the observed Hα and Hβ line-profile display no indication of structures comparable to those shown in Fig. 16. The width of the marginal ICCF structures of the observed cloud profiles is less than 100 km s^{-1}. This can be taken as hint of the width of individual emitters if they exist. This will be consistent with gas of $T_e \simeq 2\,10^4$ K and additional line broadening due to optical depth effects.

The large number of clouds, at least $N_{cl} = 10^8$, put strong constraints on discrete cloud BLR models. The confinement of the individual clouds is still the most serious problem of the discrete cloud model. The bloated star model suggested by Edwards (1980), Penston (1988), Scoville & Norman (1988), Kazanas (1989) and in a more detailed scenario proposed in a series of papers by Alexander & Netzer (1994,1997) ascribed the cold gas concentrations to the outer atmospheres or stellar winds of stars. Within the scenario presented by Alexander & Netzer detailed photoionization models, the evolution and dynamics of the central stellar cluster, and the evolution of the black hole was taken into account. They showed that the relative line intensities, the line profiles as well as the observed flux variations of the broad emission-lines can be explained by the bloated star model. But only $N_{bs} \simeq 5\,10^4$ solar mass giant stars are necessary to account for these properties. This is obviously several orders of magnitude less than the lower limit obtained by the line-profile analysis presented. Although bloated stars will solve the confinement problem in a natural way, the large discrepancy between the possible number of stars involved and the lower limit of clouds suggested by this study and the investigation on Mkn 335 and NGC 4151 (Arav et al. 1997,1998) rule out this model. However the line profiles of the bloated star population can be identified with the symmetrical, unshifted, intermediate width core component which has been suggested

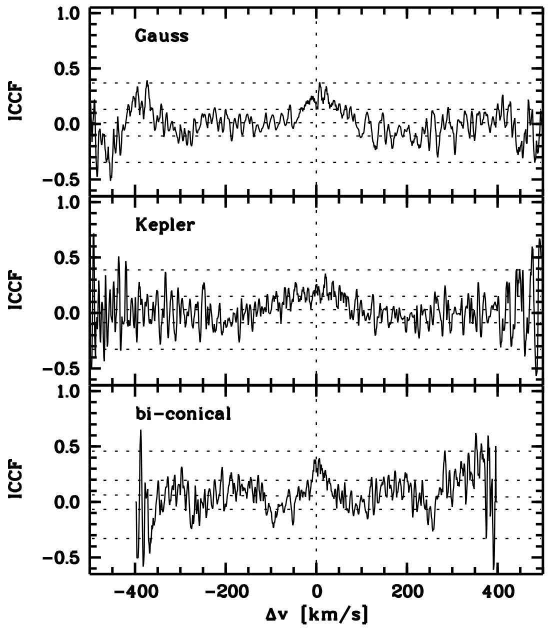

Fig. 16. The same as Fig. 15 for $N_{cl}=10^8$

by Wills et al. (1993) and Baldwin et al. (1996) in decomposition of the broad emission-line profiles.

In recent years several models based on hydromagnetically driven accretion disk winds have been suggested (e.g. Emmering et al. 1992; Bottorff et al. 1997). The line emitting gas is confined in a hydromagnetically gas flow. The line width is due to the motion of the clouds guided by the magnetic field and to electron scattering. The rotation of the magnetic field which is coupled to the accretion disk and the outflow result in a composite velocity field. The fraction of the rotational and of the outflowing component depends on the distance to the accretion disk. But also for these models individual emitting filaments should cause a detectable microstructure.

As an alternative approach several BLR models have been suggested which based on accretion disks, stellar wind and supernovae driven shocks, or hydrodynamical winds which do not lead to distributions of small individual clouds (e.g. Smith & Raine 1985, 1988; Perry & Dyson 1985; Collin-Souffrin et al. 1988; Pelletier & Pudritz 1992; Cassidy & Raine 1993; Murray & Chiang 1995, 1997; Murray et al. 1995). BLR models which ascribe the broad emission-line gas to continuous gas flows driven by a quasar wind in interaction with an accretion disk wind predicts no discrete emitters (e.g. Murray & Chiang 1995). Therefore, the result of our cross-correlation analysis provide additional indication that the broad emission-lines might be created in a continuous flow or in an accretion disk as Arav et al. (1998) pointed out.

Another important aspect of the investigation of the emission line profiles for the detection of intrinsic fluctuations is that the hypothesis of clouds has been tested so far solely for low excitation lines (LIL) like Hα or Hβ for a few AGN. But there is strong evidence for a multi-component structure fo the broad line region and the conditions for the origin of LIL and high excitation lines (HIL). Variability studies provide evidence of different response of LIL and high excitation lines (HIL) (cf. Peterson 1993) which is taken as evidence for an ionization stratification. The locally optimally emitting cloud model of Baldwin et al. (1995) suggested different locations for LIL and HIL in the density – photon flux plane. In this context the model of Perry & Dyson (1985) and Collin-Souffrin et al. (1988) indicates the necessity to study both, LIL and HIL for intrinsic microstructure. This BLR model suggests that the LIL is emitted in the outer parts of an accretion disk which is heated by reflected X-ray radiation. The HIL, on the other hand, are produced in the cooling post shock gas which is created by interaction of the quasars wind with obstacles like supernovae remnants in the close environment of the central engine. In this scenario the kinematics of the line emitting material of LIL and HIL is different and is in good agreement with the observed blueshift of the order of $\Delta v \approx 1000$ km s^{-1} of HIL profiles with respect to LIL profiles (e.g. Crenshaw 1986). Hence, it might be possible that the LIL are emitted from a disk like structure e.g. an accretion disk (cf. Collin-Souffrin et al. 1988) while the HIL are dominated by discrete emitters like gas in a hydromagnetically driven wind. In this case LIL like Hα and Hβ would show no intrinsic fluctuations. Therefore, future investigations should focus on emission-line profiles of HIL like CIV 1548 and CIII] 1909 to test the hypothesis that these emission lines might originate in discrete emitters in contrast to the LIL.

6. Conclusions

We observed high S/N echelle spectra of the quasar 3C 273 with a spectral resolution of 10 km s^{-1} to search for intrinsic fluctuations.

A finite number of individual clouds in the broad-line region will cause characteristic microstructures in the line profiles which can be detected especially in the outer wings.

The residua of the profile wings of the Hα and Hβ emission-lines were studied using cross-correlation methods. No significant ICCF signal was detected above a 3-σ threshold correlating Hα vs. Hβ as well as Hα vs. Hα and Hβ vs. Hβ.

We studied several simplified models for the cloud distribution, the velocity field, and the line width of an individual cloud to estimate a lower limit for the number of clouds which can be hidden in a line profile. The comparison of the model simulation results indicates that the number of emitters is larger than $N_{cl} = 10^8$ assuming a FWHM$\simeq$15 km s^{-1} for an individual cloud, i.e. the profile width is caused entirely by thermal broadening. But the number of clouds might be of the order of $N_{cl} \simeq 10^8$ if the width of an discrete emitter is of the order of 100 km s^{-1}. The additional line broadening might be due to optical depth effects or electron scattering. The non-detection of an ICCF signal and also the results of Arav et al. (1997, 1998) provides evidence that bloated star models can be ruled out as dominant source for the line emitting cloud population if only solar mass giant stars are taken into account. Although, the models we applied to estimate a lower limit of the number of clouds based on simple assumptions and were restricted to structures with FWHM $\leq 200\ \mathrm{km\,s^{-1}}$ the number of individual emitters has to be of the order of 10^8 or more. However, models which are based on non-discrete emitters, i.e. accretions-disk emission or emission from a continuous flow are compatible with the non-detection of a cross-correlation signal.

References

Alexander, T. & Netzer, H. 1994, MNRAS, 270, 803
Alexander, T. & Netzer, H. 1997, MNRAS, 284, 967
Arav, N., Barlow, T.A., Laor, A., & Blandford, R.D. 1997, MNRAS, 288, 1015
Arav, N., Barlow, T.A., Laor, A., Sargent, W.L.W., & Blandford, R.D. 1998, MNRAS, 297, 990
Atwood, B., Baldwin, J.A., & Carswell, R.F. 1982, ApJ, 257, 559
Baldwin, J.A., Ferland, G.J., Korista, K.T., & Verner, D. 1995, ApJ, 455, L119
Baldwin, J.A., Ferland, G.J., Korista, K.T., et al. 1996, ApJ, 461, 664
Blandford, R.D. & Rees, M.J. 1992, in 'Testing the AGN Paradigm', eds. S.S. Holt, S.G. Neff, & C.M. Urry, AIP Conf. Proc. 254, 3
Bottorff, M., Korista, K.T., Shlosman, I., & Blandford, R.D. 1997, ApJ, 479, 200
Bradley, S.E. & Puetter, R.C. 1986, A&A, 165, 31
Capriotti, E., Foltz, C., & Byard, P. 1981, ApJ, 245, 386
Cassidy, I. & Raine, D.J. 1993, MNRAS, 260, 385
Collin-Souffrin, S., Dyson, J.E., McDowell, J.C., & Perry, J.J. 1988, MNRAS, 232, 539
Crenshaw, D.M. 1986, ApJS, 62, 821
Davidson, K. & Netzer, H. 1979, in Rev. Mod. Phys., 51, 737
Edwards, A.C. 1980, MNRAS, 198, 757
Emmering, R.T., Blandford, R.D., & Shlosman, I. 1992, ApJ, 385, 460
Ferland, G.J. & Persson, S.E. 1989, ApJ, 347, 656
Ferland, G.J., Peterson, B.M., Horne, K., Welsh, W.F., & Nahar, S.N. 1992, ApJ, 387, 95
Gaskell, C.M. & Peterson, B.M. 1987, ApJS, 65, 1
Harms, R.J. et al. 1994, ApJ, 435, L35
Hubbard, E.N. & Puetter, R.C. 1983, ApJ, 265, 35
Kazanas, D. 1989, ApJ, 347, 74
Krolik, J.H., McKee, C.F., & Tarter, C.B. 1981, ApJ, 249, 422
Krolik, J.H. 1999, Active Galactic Nuclei, Princeton Series in Astrophysics
Murray, N., Chiang, J., Grossman, S., & Voit, G.M. 1995, ApJ, 451, 498
Murray, N. & Chiang, J. 1995, ApJ, 454, L105
Murray, N. & Chiang, J. 1997, ApJ, 474, 91
Netzer, H. 1990, in Saas-Fee Advanced Course 20: Active Galactic Nuclei, eds. R.D. Blandford, H. Netzer, & L. Woltjer, (New York, Springer), 57
Norman, C. & Scoville, N. 1988, ApJ, 332, 124
Osterbrock, D.E. & Martel, A. 1992, PASP, 104, 76
Osterbrock, D.E. 1993, ApJ, 404, 551
Osterbrock, D.E., Fulbright, J.P., Martel, A., Keane, M.J., & Trager, S.C. 1996, PASP, 108, 277
Pelletier, G. & Pudritz, R.E. 1992, ApJ, 394, 117
Penston, M.V. 1988, MNRAS, 233, 601
Perry, J.J. & Dyson, J.E. 1985, MNRAS, 213, 665
Peterson, B.M. 1993, PASP, 105, 247
Peterson, B.M. 1997, An Introduction to Active Galactic Nuclei, Cambridge University Press
Rees, M.J. 1987, MNRAS, 228, 47p
Sargent, W.L.W., Young, P.J., Boksenberg, A. et al. 1978, ApJ, 221, 731
Schmid, H.-M., Krautter, J., Appenzeller, I., et al. 1999, A&A, submitted
Scoville, N. & Norman, C. 1988, ApJ, 332, 163
Smith, M.D. & Raine, D.J. 1985, MNRAS, 212, 425
Smith, M.D. & Raine, D.J. 1988, MNRAS, 234, 297
Tonry, J. & Davis, M. 1979 AJ, 84, 1511
White, R.J. & Peterson, B.M. 1994, PASP, 106, 879
Wills, B.J., Brotherton, M.S., Fang, D., et al. 1993, ApJ, 415, 563

Acknowledgements. This work has been supported by DFG grant Sonderforschungsbereich 328.

This article was processed by the author using Springer-Verlag LaTeX A&A style file *L-AA* version 3.